Temperature Diagnostics for Field-Reversed Configuration Plasmas on the Pulsed High Density (PHD) Experiment

Hiroshi GOTA, Samuel ANDREASON, George VOTROUBEK, Chris PIHL and John SLOUGH
Plasma Dynamics Laboratory, University of Washington, Seattle, WA 98195, USA

(Received 3 December 2006 / Accepted 13 March 2007)

The high flux source for the Pulsed High Density Experiment (PHDX) has been constructed, and field-reversed configuration (FRC) plasmas are being produced. To diagnose FRC plasma temperatures three kinds of diagnostic systems have been set up on PHDX; $\lambda = 632.8$ nm He-Ne laser interferometer system at the midplane for total temperatureT_{total}, 16 channel spectrometer for ion temperature T_i and soft x-ray (SXR) measurement system for electron temperature T_e viewed along z-axis, respectively. The SXR measurement system consists of five sets of collimators and AXUV100 photodiodes with directly deposited filters which have different bandpass regions. As a result of preliminary temperature diagnostics, the following plasma parameters are estimated during a relatively quiescent phase of FRCs; $T_{total} \sim 50$ eV, $T_i \sim 50$ eV and $T_e \sim 25$ eV. This result does not agree with the equilibrium relation of $T_{total} \approx T_i + T_e$, and it must be caused by plasma condition and our assumptions in the spectral analysis.

Keywords: field-reversed configuration, FRC, theta pinch, compact torus, temperature diagnostics, soft x-ray

DOI: 10.1585/pfr.2.S1050

1. Introduction

A field-reversed configuration (FRC) is one of the simplest toroidal plasma configurations [1]. The FRC plasma is confined within a separatrix by a poloidal magnetic field that is generated by plasma diamagnetic toroidal currents, and has negligible toroidal field. There are many advantages of FRC plasmas including its compact, simple geometry, high plasma beta, and ease of linear translation. The Pulsed High Density Experiment (PHDX) will expand the conventional regime of the FRC to the very compact, high energy density regime to approach fusion. In this approach, the energy needed to compress the FRC to fusion conditions is transferred to the FRC via simple, relatively low field acceleration and compression coils. The High Flux Source (HFS) of PHDX is designed to enable the completion of scaling and confinement studies by enabling the ability to program FRC elongation. The experiment is essentially the first step towards breakeven, and continuing progress can be made in incremental steps with additional stages of acceleration and compression. The ultimate goal of PHDX is to form, accelerate and compress the FRC to a density of 1×10^{23} m^{-3} at a temperature greater than 1 keV. Following energy confinement time, τ_E, predicted by previous FRC scaling, the resulting FRC should attain an $n\tau_E$ product of $\sim 5 \times 10^{18}$ m^{-3}s, where n is a plasma density.

Plasma temperatures are determined by commonly using a He-Ne laser interferometer system for not only FRCs but other configurations including compact tori, tokamaks, and similar devices. In PHDX, a $\lambda = 632.8$ nm He-Ne laser interferometer system is installed to measure the line-integrated electron density, $\int n_e dl$, and estimate the total temperature, T_{total}, of FRC plasmas. For discussing detailed temperature analysis, the impurity measurement of plasma is widely used on many experimental devices. A 16 channel spectrometer manufactured by SPEX Industries has been set up on the HFS to estimate the velocity, v, and ion temperature, T_i, of FRCs by measuring the Doppler shift and broadening of impurity species; this spectrometer has a 16 element Hamamatsu R5900U series photomultiplier tube (PMT) for light detection. In addition, a soft x-ray (SXR) measurement [2, 3] system has recently been developed on the HFS to estimate electron density, n_e, and temperature, T_e, of FRCs. Both parameters of n_e and T_e are approximately determined by comparing the response of the several filtered detectors to their computed response using the emissivity from an atomic model of the plasma with T_e convolved with the spectral responsivity of each detector.

For detecting the SXR radiation from the FRC plasma, AXUV100 photodiodes, manufactured by International Radiation Detectors (IRD) [4], are used. There are many features of AXUV photodiode which makes it well suited for this diagnostic: coverage of the complete photon spectral range (0.04-1100 nm), and having no doped dead-region on the detector surface resulting in quantum efficiencies near theoretical limits for XUV photons and other low energy particles. In PHDX we developed five sets of AXUV100 photodiodes and filters, which have different bandpass characteristics and are already deposited on each

author's e-mail: gota@u.washington.edu

diode, respectively. The simplest approach to analyzing the SXR data would be to try to reconstruct the SXR spectrum from the several SXR measurements at each time point; then, spectrum could be compared to ideal spectra generated by bremsstrahlung emission formula or spectral analysis code. If the reconstructed spectrum has enough detail, the fruit of this comparison would be dynamic values for plasma temperature and impurity content. To estimate the sample spectrum on PHDX, PrismSPECT (spectral analysis code from the Prism Computational Science, Inc.) is used. Once we have an emissivity for some nominal choice of impurities, we can use simple scaling with impurity density to assemble an emissivity spectrum for a combination of impurities.

In the following section the experimental setup including basic diagnostics and three kinds of temperature diagnostic systems of the PHDX are described. In section 3, experimental results from all temperature diagnostics are compared and discussed.

2. Experimental Setup

2.1 Diagnostics for the PHDX

In the source section of the PHDX shown in Fig. 1 (a), a 2.6-m long and 0.8-m diameter silica tube is used. To produce the preionization plasmas inside the tube two kinds of preionization method are used; axial discharge and magneto plasma dynamic (MPD). They provide much higher lift-off flux than in a ringing-θ field preionization setup. The axial magnet coils are individual, electrically insulated copper coils and wrapped just outside the quartz tube; each coil has 15-cm width and 3-mm thickness with a coil spacing of 25 cm. Two of 9 coils located at both ends produce bias field with the others used for fast-reversal field; the bias and reversal fields are 0.06 T and 0.2 T at peak, respectively.

To diagnose the FRC plasma temperatures, three kinds

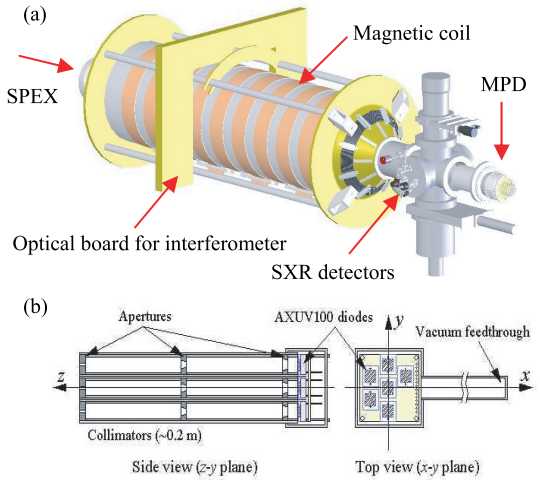

Fig. 1 Schematics of the PHDX: (a) high flux source, and (b) soft x-ray detector.

of diagnostic systems have been set up on HFS; λ = 632.8 nm He-Ne laser interferometer system at the midplane of the HFS, 16 channel spectrometer installed for end-on viewing, and SXR measurement system mounted on the end flange viewing along z-axis. Other diagnostic systems for the HFS of PHDX are: 9 pairs of magnetic loops and flux loops installed underneath each copper coil are used for determining the separatrix radius, shape and energy of the FRC plasmas; 14 channels of visible light measurement (unfiltered Si-Photodiode) covering 4 radial locations from the end and 10 axial locations along the length have been installed for analyzing preionization efficiency and uniformity as well as FRC formation dynamics; a gated spectrometer for detecting impurity line spectra is installed; a bolometer system is set up at the end flange viewing along the z-axis to measure the total radiated power of FRCs; an end-on fast framing camera (IMACON) and a charge-coupled device camera are installed and in use. A 64 channel array system of visible bremsstrahlung tomography is available, and detailed information about this system is described in previous work [5].

2.2 He-Ne laser interferometer

An acousto-optic modulator (AOM) is used to split the 5 mW He-Ne laser beam into reference and scene beams, which also induces a 40 MHz phase-shift on the deflected beam, here the reference beam. The scene beam passes through the quartz tube at the midplane and zero impact parameter, is reflected by a return mirror on the far side of the HFS, and returns through almost the same position. The beams are recombined at a beam splitter and band-pass filtered ($\lambda \sim 632$ nm and FWHM~10 nm filter), and monitored with a detector consisting of a collimator, plastic optical fiber and photodiode. The quadrature electronics compare the phase of the original 40 MHz local oscillator with the 40 MHz signal that was added to the laser beam by the AOM, removing ambiguities in phase information. The phase shift is related to the electron density by the relation

$$\Delta\phi = \frac{\omega}{2cn_c}\int n_e dl, \tag{1}$$

where ω is related to the frequency of light by $\omega = 2\pi c/\lambda$ and n_c is the cut off density at which light at wavelength λ will encounter an optically thick plasma and will not penetrate, $n_c = \omega^2 m\varepsilon_0/e^2$. The phase shift is easily measured using this technique, and an electron density along the path of the laser found. This system has a sensitivity to plasma electron density of $\int n_e dl = 3.53 \times 10^{21}\,\mathrm{m}^{-2}$ per fringe. Total temperature of FRCs is estimated by using pressure balance relations:

$$T_{total} = \frac{B_{ext}^2}{2\mu_0 n_e e}\left(1 - \frac{1}{2}x_s^2\right), \tag{2}$$

where B_{ext} is an external field and x_s is the ratio of separatrix radius to coil radius; then, the term of $(1 - x_s^2/2)$ indicates separatrix beta, β_s. Here, we assume n_e equals to averaged electron density $< n_e >$.

2.3 Sixteen channel spectrometer

Plasma emission is focused through a 2 μm entrance slit and detected by a 16 ch PMT array. This detector has a UV window that provides good sensitivity from 185-650 nm. Each channel of the PMT is recorded on a digitizer and provides a time-resolved record of the spectra. The overall resolution of the instrument is ~0.036 nm. For calibrating the intensity of 16 ch PMT detector with −800 V supply voltage, a mercury pencil lamp is used and the detected wavelength compared with Hg I lines from the National Institute of Standards and Technology (NIST) Atomic Spectra Database.

The ion temperature of FRC plasma is measured in terms of the Doppler broadening. Under the assumption of a thermal Maxwellian velocity distribution, the Doppler broadened spectral line shape of the transition is expressed by a Gaussian profile

$$I(\lambda) \sim \exp\left[-(\Delta\lambda/\Delta\lambda_D)^2\right], \tag{3}$$

with the full width at half maximum

$$\Delta\lambda_{FWHM} = 2(\ln 2)^{1/2}\Delta\lambda_D = 7.71\times10^{-5}\lambda(T_i/M)^{1/2}, \tag{4}$$

where T_i is in eV, $\Delta\lambda_D$ centered at the wavelength of the observed spectra λ, and M is the ion mass in atomic units. This half-width and thus the corresponding apparent temperature must be corrected by taking into account the Zeeman and Stark effects. With these corrections taken into account, the measured Doppler broadening is used to solve for T_i.

2.4 Soft x-ray measurement system

The SXR measurement system consists of collimators including 3 different sizes of apertures ($\phi \sim 2$, 5 and 8 mm) and 5 sets of AXUV100 photodiodes (sensitive area of $10\times10\,\mathrm{mm}^2$) with directly deposited filters: single filter of 150-nm Al, multifilters of 200-nm Zr and 50-nm C, 200-nm Ti and 100-nm Pd, 200-nm Sn and 10-nm Ge, and 60-nm Cr and 150-nm Al. Schematics of the SXR measurement system is illustrated in Fig. 1 (b). A quantum efficiency of each filtered AXUV100 photodiode taken from the IRD website [4] is shown in Fig. 2, along with a sample spectrum from PHDX. To increase the uniformity of detector signal we supply 3 volts of a reverse bias using batteries, and 150 Ω of a load resistance is used as a termination.

The emissivity of SXRs can be determined either from a bremsstrahlung formula or using a spectral analysis code. To estimate the detector signal, we can numerically integrate the bremsstrahlung formula over photon energy E and along the detector line of sight l, taking into account the quantum efficiency of filtered detector:

$$I_{\mathrm{det}} \propto \int_l \int_E n_e^2(l)T_e^{-1/2}(l) \times \exp(-E/T_e(l))S(E)I(E,l)\mathrm{d}E\mathrm{d}l, \tag{5}$$

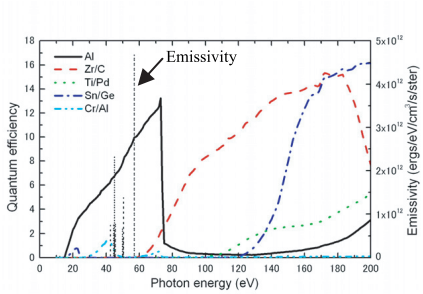

Fig. 2 Quantum efficiency of filtered AXUV100 photodiode, and sample spectrum on the PHDX.

where S and I represent the quantum efficiency and the intensity of impurity line, respectively. Meanwhile the PrismSPECT can easily determine the plasma emissivity under the assumption of density and temperature with some nominal choice of impurities. In our T_e analysis we use this software to compare the signal of SXR detector with calculated response. FRC is predominantly Deuterium plasma in PHDX, but with the following impurities: 0.25 % Carbon, 0.5 % Oxygen, and 0.1 % Silicon. Furthermore, we assume several calculational conditions such as time-independent, non-local thermal equilibrium (collisional radiative equilibrium) ionization and level population calculation, and with optically thin radiation transport. Sample spectrum of emissivity under the conditions of $T_e \sim 50$ eV and $n \sim 3\times10^{21}\,\mathrm{m}^{-3}$ is shown in Fig. 2. In a given spectrum a small number of strong lines dominate, and a single element can completely dominate the emission; dominant impurity line, for instance, is Oxygen at 10 eV and Silicon at 50 eV. Impurity lines dominate over continuum, and note that the continuum is dominated by recombination, rather than free-free emission.

3. Experimental Results on the HFS

FRC plasmas are produced by a field-reversed theta-pinch method with 10 mTorr Deuterium. Figure 3 shows the time sequence of the external field B_{ext}, excluded flux radius $r_{\Delta\phi}$, and line-integrated electron density $\int n_e dl$ at the midplane of HFS, respectively. Plasma parameters at relative quiescent phase ($t \sim 15$ μs) are as follows: $r_{\Delta\phi} \sim 0.2$ m, averaged electron density $<n_e> \sim 2.0\times10^{21}\,\mathrm{m}^{-3}$, and configuration life time $\tau_\phi \sim$ 40-50 μs.

SXR signals of all five filtered-diodes are shown in Fig. 4 (a), and then each signal is subtracted by that of a vacuum reference. Since the Al filter has wideband and high transmission at low photon energy region, peak current of the diode is approximately 11 mA ($t \sim 22$ μs); at the same time the results of Zr/C- and Sn/Ge-filtered diodes are 4.0 and 1.5 mA, respectively, and the others are approximately 1.0 mA. Note that we assume each detector measures the same plasma conditions (density and temperature profiles) and line of sight. Here we can obtain the

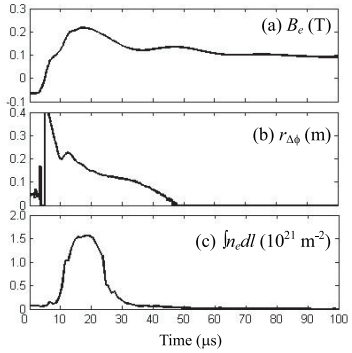

Fig. 3 Time sequence of (a) external field, (b) excluded flux radius, and (c) line-integrated electron density.

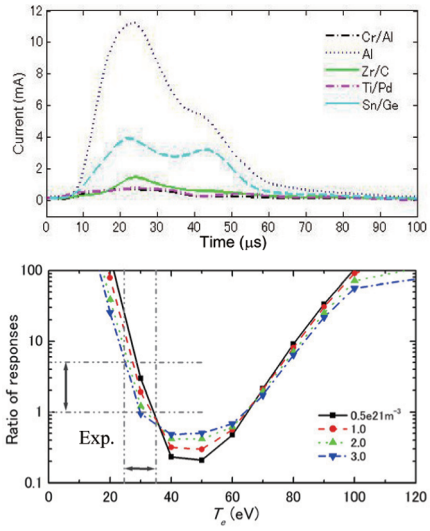

Fig. 4 (a) Time sequence of detector signals, and (b) calculated ratio of Sn/Ge- to Zr/C-filtered responses and the predictable consequence from the experiment.

ratios of several choices of signal combination and time point. To compare the ratios of several responses between experiment and simulation, the PrismSPECT is carried out under the plasma conditions of $n \sim 0.5\text{-}3.0 \times 10^{21}$ m^{-3} and $T_e \sim 10\text{-}200$ eV. As results of integrating the emissivity over photon energy with taking into account the quantum efficiency of five different filtered-diodes at each simulation, the ratio of responses as a function of electron temperature are obtained; sample results of ratio of Sn/Ge- to Zr/C-filtered responses are shown in Fig. 4 (b). To estimate T_e in our analysis plasma density is determined by the interferometer system, and then we compare the responses from both experiment and simulation. At $t = 22$ μs, for example, the ratio of Sn/Ge to Zr/C signals is 2.7 and plasma density is 2.5×10^{21} m^{-3}, and then T_e is approximately estimated at 30±2 eV from Fig. 4 (b).

Figure 5 shows the time sequence of FRC plasma temperatures resulting from all three diagnostics as discussed above. Using Eq. (2) and plasma parameters shown

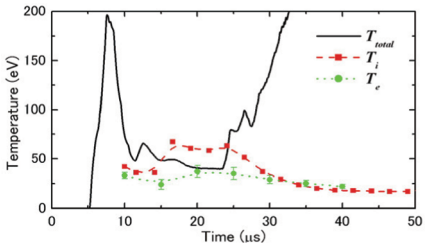

Fig. 5 Experimental results from all temperature diagnostics on PHDX.

in Fig. (3), time evolution of T_{total} is easily estimated; T_{total} stays around 50 eV till $t = 24$ μs, but is steeply increased because of decreasing the electron density. Results from the Doppler broadening measurement (CIII line at $\lambda = 229.69$ nm) indicate ion temperature of FRC plasma to be $T_i \sim 30$ eV at the beginning of axial contraction and increased up to 70 eV. Finally, preliminary results of T_e estimation using the SXR measurement system are seen in the same figure; T_e remains in the range of 25-35 eV. Since this estimation is carried out under several assumptions in both experiment and simulation, we should be careful of comparing T_e result with the others. The problem with this T_e estimation, for example, is that if there is a time-dependent density, then from looking at the SXR signals alone, we cannot say whether a changing signal is from a changing temperature or a changing density. Total temperature of FRC plasma can be determined by the sum of T_i and T_e, however the result of Fig. 5 indicates $T_{total} < T_i + T_e$ at a relatively quiescent phase (15-24 μs); especially high T_i. We presume this must be caused by both the condition of FRC plasma (shape, position, equilibrium and life time) and the location of the spectrometer (end-on viewing).

In summary the preliminary experimental results from all three temperature diagnostics for FRC plasmas are $T_{total} \sim 50$ eV, $T_i \sim 50$ eV, and $T_e \sim 25$±2 eV at $t = 15$ μs. They do not indicate the equilibrium relation, $T_{total} \neq T_i + T_e$, and we presume that FRC plasma is not sustained equilibrium. For future iterations we will change the location of spectrometer, fractions of impurity on HFS, and our assumptions of the plasma condition.

Acknowledgments

Authors would like to thank Profs. M. Brown and D. Cohen in Swarthmore College for helping us set up the soft x-ray measurement system. This research was funded by the United States Department of Energy, Office of Fusion Energy Sciences.

[1] M. Tuszewski, Nucl. Fusion **28**, 2033 (1988).
[2] F.C. Jahoda *et al.*, Phys. Rev. **119**, 843 (1960).
[3] J. Kiraly *et al.*, Nucl. Fusion **27**, 397 (1987).
[4] International Radiation Detectors (http://www.ird-inc.com).
[5] H. Gota *et al.*, Rev. Sci. Instrum. **77**, 10F319 (2006).